Eur. Phys. J. Spec. Top. (2021) 230:567–577
https://doi.org/10.1140/epjs/s11734-021-00008-0

THE EUROPEAN PHYSICAL JOURNAL SPECIAL TOPICS

Review

Pairing in pure neutron matter

S. Ramanan[1,a] and M. Urban[2,b]

[1] Department of Physics, Indian Institute of Technology Madras, Chennai 600036, India
[2] Université Paris-Saclay, CNRS-IN2P3, IJCLab, 91405 Orsay Cedex, France

Received 19 October 2020 / Accepted 23 December 2020 / Published online 1 April 2021

Abstract We review the long standing problem of superfluid pairing in pure neutron matter. For the s-wave pairing, we summarize the state of the art of many-body approaches including different nn interactions, medium polarization, short-range correlations and BCS–BEC crossover effects, and compare them with quantum Monte Carlo results at low densities. We also address pairing in the p-wave, which appears at higher densities and, hence, has large uncertainties due to the poorly constrained interactions, medium effects and many-body forces.

1 Introduction

Superfluiditity in nuclei is nearly a 60-year-old problem. However, a satisfactory microscopic description of the phenomenon continues to remain a challenge as the problem is marred by uncertainties in the input interactions, both at the few body level and the medium corrections. The possibility of neutron superfluidity was already pointed out around 1960 [1–3]. The observational confirmation began with the discovery of pulsars [4], their connection to rotating neutron stars [5] and the subsequent observation of glitches in the period of rotation of these pulsars. Rotating neutron stars are almost perfect clocks with a period of rotation that increases very slowly with time. However, sometimes, the period of rotation suddenly decreases, followed by long relaxation times (over years) before it returns to its pre-glitch value. Such glitches can be explained if one allows for the existence of a superfluid phase in the inner crust of the star through the mechanism of vortex unpinning [6,7] (maybe one needs also superfluidity in the core [8]). Further, the existence of a superfluid state is crucial to explain the observational data on cooling [9–11].

The two-body interaction between two neutrons has attractive components and while it is not sufficient to produce a bound di-neutron state in free space, in the presence of other neutrons, this attraction leads to Cooper instability leading to the existence of a superfluid phase with s-wave pairing, which typically exists in the inner crust of neutron stars. The NN interaction is attractive in the spin triplet state as well that leads to p-wave pairing, and such a phase is assumed to exist at higher densities in the outer layers of the core of the star.

In addition to the physics of neutron star crusts, pairing plays a crucial role in finite nuclei as well by contributing to extra binding, for example the extra binding leading to an energy gap in even–even nuclei compared to the quasi-particle spectrum of odd-A nuclei or the even–odd staggering in binding energy [12,13]. Close to the drip lines, large even–odd-staggering has been observed in isotopes of C, Ne and Mg [14–16].

In the literature, several extensive reviews already exist on the subject of neutron star physics and superfluidity in both finite and infinite systems [17–20]. In the present special topics issue, we aim to give a short overview of the status of s-wave pairing, in particular screening and beyond-BCS crossover effects, and of the outstanding questions of p-wave pairing.

2 Singlet pairing

2.1 BCS gap equation

In the case of an attractive interaction between fermions, the filled Fermi sea becomes unstable with respect to the formation of Cooper pairs. The starting point to study pairing is the BCS theory, where the gap or the critical temperature is given by the BCS gap equation, which in the s-wave spin-singlet ($^1S_0$) channel is given by [21]:

$$\Delta(k) = -\frac{1}{\pi}\int_0^\infty dk'\, k'^2\, V(k,k')\frac{\Delta(k')\tanh\left(\frac{E(k')}{2T}\right)}{E(k')}, \quad (1)$$

[a] e-mail: suna@physics.iitm.ac.in (corresponding author)
[b] e-mail: michael.urban@ijclab.in2p3.fr

where $\Delta(k)$ is the momentum-dependent gap, $V(k,k')$ is the matrix element of the s-wave neutron–neutron (nn) interaction, $E(k) = \sqrt{\xi^2(k) + \Delta^2(k)}$ is the quasiparticle energy with $\xi(k) = \varepsilon(k) - \mu$ and $\varepsilon(k) = k^2/(2m^*)$, m^* is the neutron effective mass, T the temperature and μ the chemical potential (including the mean-field energy shift). The critical temperature T_c is the highest temperature at which there is a non-trivial solution for Eq. (1). At $T = T_c$, the gap in $E(k')$ can be neglected and as a result Eq. (1) becomes a linear eigenvalue equation. In the weak-coupling limit where $\Delta(k_F) \ll \mu$, the gap at zero temperature is related to the BCS transition temperature by $T_c = 0.57\,\Delta_{T=0}(k_F)$. In the case of neutron matter, this formula is a good approximation at all values of μ, because the Fermi surface remains rather well defined. To simplify the notation, we will from now on write $\Delta = \Delta(k_F)$.

In our calculations, we mostly use the renormalization group (RG) based interactions, $V_{\mathrm{low}\,k}$ [22] and V_{srg} [23]. They have an inherent scale (Λ for $V_{\mathrm{low}\,k}$ and λ for V_{srg}) that sets the scale of decoupling between the low and high momenta. Such a scale is arbitrary and observables should be independent of this scale. Within the simplest BCS approximation, i.e., employing the free-space nn interaction $V^0(k,k')$ and the free neutron mass $m^* = m$, any realistic nn interaction that reproduces the two-body neutron phase shifts yields the same BCS gap [24].

However, uncertainties arise already at the BCS level as soon as the effective mass $m^* \neq m$ is included, since this affects the density of states $N_0 = m^* k_F/\pi^2$, where $k_F = (3\pi^2 n)^{1/3}$ is the Fermi momentum with n the number density. Recent quantum Monte Carlo (QMC) calculations [25] found that the neutron effective mass drops only moderately with increasing density, similar to what one gets with effective Gogny forces [26,27], while effective Skyrme interactions of the Saclay-Lyon family [28] predict a stronger drop, in contrast to those of the Bruxelles-Montreal family [29,30] which predict a slightly increasing effective mass. In particular at higher densities beyond $k_F \approx 0.8$ fm^{-1} (corresponding to number densities above 0.017 fm^{-3} or mass densities above 2.9×10^{13} g/cm^3), where the BCS gap is maximum, the gap depends very sensitively on the density of states, and, therefore, the different effective masses lead to sizable uncertainties as can be seen in Fig. 1.

At lower densities, the effective mass is close to the free one, and the gap is less sensitive to it. In this region, the uncertainties come mainly from corrections beyond the BCS approximation. These will be addressed in the following subsections.

2.2 Screening corrections

It is well known that corrections beyond the BCS approximation due to density and spin-density fluctuations that the neutrons create in the surrounding medium are very important. Such corrections are called medium polarization or screening effects, since they are

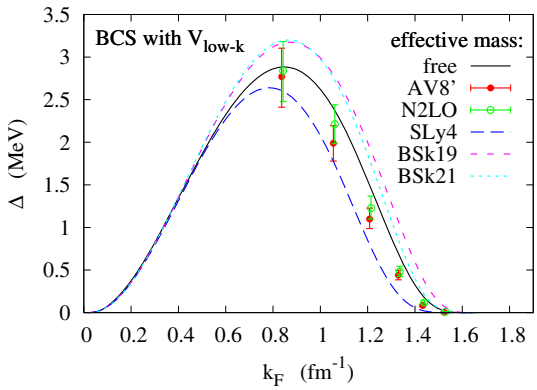

Fig. 1 BCS pairing gaps $\Delta = \Delta(k_F)$ obtained from Eq. (1) using the $V_{\mathrm{low}\,k}$ interaction (with a cutoff of $\Lambda = 2\mathrm{fm}^{-1}$) [22,23], as functions of k_F. The differences between the results are only due to the different effective masses m^* used in the calculations: free mass ($m^* = m$, black solid line), effective masses from recent auxiliary-field diffusion Monte-Carlo calculations [25] using the AV8′+UIX interaction (red filled circles) and the chiral N2LO interaction (green empty circles), and effective masses from three different Skyrme parametrizations: SLy4 [28] (blue long dashes), BSk19 and BSk21 [30] (purple short dashes and turquoise dots, respectively)

analogous to the screening of the Coulomb interaction. They can be taken into account in the gap equation by adding the induced interaction to the bare nn interaction, so that,

$$V(k,k') = V^0(k,k') + V^{(a)}(k,k') + V^{(b)}(k,k') \ , \quad (2)$$

where the induced interactions, $V^{(a)}$ and $V^{(b)}$, are as seen in Fig. 2. In this figure, diagram (a) allows for one particle-hole (ph) bubble insertion while diagram (b) sums the ph bubble series (random-phase approximation, RPA, represented by wavy lines). In these diagrams, the interaction $\tilde{V}$ shown by the dotted lines is meant to be antisymmetrized, $\langle 12|\tilde{V}|34\rangle = \langle 12|V|34\rangle - \langle 12|V|43\rangle$, i.e., it includes also the exchange graphs which are not drawn.

There have been many attempts to calculate the induced interactions in the literature [32–38]. Especially the earlier calculations [32,33] found an extremely strong suppression of the gap. However, since the work by Cao et al. [36], a consensus seems to emerge that the gap is not too strongly reduced. This is shown in Fig. 3 which summarizes more recent screening and QMC results. In Fig. 3b, we also show the result $\Delta/\Delta_{\mathrm{BCS}} = (4e)^{-1/3} \approx 0.45$ (black star) obtained long ago by Gor'kov and Melik-Barkhudarov (GMB) [31], which should become valid in the limit $|k_F a_{nn}| \ll 1$, with $a_{nn} \approx -18.5$ fm the nn scattering length.

It is seen that the two screening calculations [36,38] do not quite agree with each other. We will come back to a more detailed discussion of these calculations below. The QMC calculations, which are supposed to be, up to numerical limitations, exact solutions of the many-

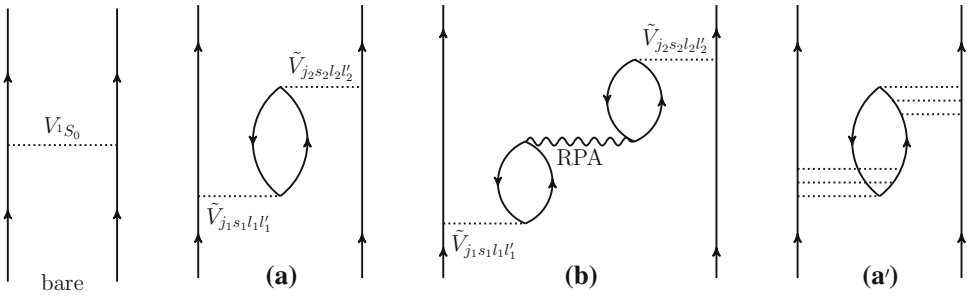

Fig. 2 In the medium, the bare pairing interaction (leftmost diagram) is modified by the screening corrections (**a**) and (**b**). Diagram (a′) illustrates the resummation of ladders in the 3p1h vertices of diagram (**a**) implicitly assumed in the derivation of the GMB result [31]

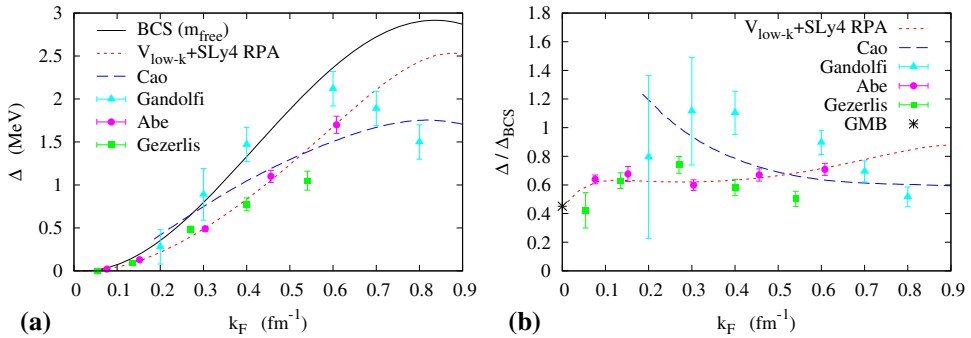

Fig. 3 **a** Screening and QMC results for the gap in neutron matter as a function of the Fermi momentum k_F. The blue dashes and red dots are the final results of the screening calculations of Cao et al. [36] and of our own work [38], respectively. The turquoise triangles, purple points, and green squares are QMC results of Gandolfi et al. [39], Abe and Seki [40], and Gezerlis and Carlson [41], respectively. For comparison, the BCS result Δ_{BCS} obtained without effective mass is shown as the black line (same as in Fig. 1). **b** Same data as in **a** but normalized to Δ_{BCS}. The GMB result [31] is shown as the black star

body problem, show only a moderate suppression. The gaps of Ref. [39] (turquoise triangles), were obtained with the auxiliary-field diffusion Monte Carlo technique using the Argonne V8′ *nn* interaction (AV8′) and the Urbana IX three-body force (UIX) and is not significantly reduced compared to Δ_{BCS} up to $k_F \sim 0.6$ fm^{-1}, but the error bars are huge. The purple points of Ref. [40] were obtained within a method based on the discretization of the Hamiltonian on a lattice (determinantal quantum Monte Carlo). The interaction used in this calculation is much simpler, as it includes only the leading and next-to-leading orders (NLO) of pionless effective field theory (EFT), and is only valid at low momenta, i.e., low densities. These gaps are reduced by an almost constant factor of about 0.6–0.7 compared to Δ_{BCS} (see Fig. 3b). The almost perfect agreement of these results with the red dashed curve is probably accidental. A similar behavior was found in Ref. [41] using the AV4 interaction within the variational and subsequent Green's function Monte-Carlo method. At very low densities, these results tend (within the error bars) towards the GMB limit. According to Ref. [41], the discrepancy between Refs. [39] and [41] might be due to the less optimized wave function used in Ref. [39].

Let us now discuss in some more detail the screening calculations. In Fig. 4, we display again the ratios of screened gaps to our reference curve Δ_{BCS} which is the BCS gap with the free neutron mass (black solid line in Fig. 1), including the results obtained at intermediate steps on the way to the final results. Figure 4a summarizes the neutron-matter results of Ref. [36]. In that work, the 3p1h vertices $\tilde{V}$ (dotted lines in Fig. 2) are the Brückner G matrix. Up to the projection on the $^1S_0$ wave, diagram (a) can be schematically written as

$$V^{(a)} = \frac{\pi}{2} \sum_{\mathbf{p}\sigma} \tilde{V} \, \frac{n(\mathbf{p}-\frac{\mathbf{q}}{2}) - n(\mathbf{p}+\frac{\mathbf{q}}{2})}{\varepsilon\left(\mathbf{p}+\frac{\mathbf{q}}{2}\right) - \varepsilon\left(\mathbf{p}-\frac{\mathbf{q}}{2}\right)} \, \tilde{V} \,, \qquad (3)$$

where we have omitted all momentum and spin labels of $\tilde{V}$. Here, $\mathbf{p}$ and σ are the momentum and spin labels that are summed over in the ph loop and $\mathbf{q} = \mathbf{k} - \mathbf{k}'$ is the momentum transfer. The occupation numbers can be safely approximated by step functions $n(\mathbf{p}) = \theta(k_F - |\mathbf{p}|)$. Also, as it is usually done, the static approximation is made, i.e., the energy transfer in the ph bubble is neglected. To simplify this complicated expression, the authors of Ref. [36] replaced $\tilde{V}$ by its average value $\langle \tilde{V} \rangle$, where the averaging is done around the Fermi surface, so that it could be taken out of the sum, which then

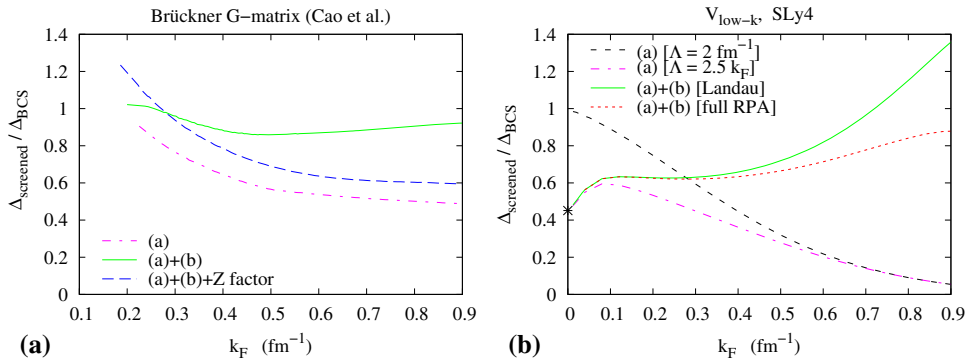

Fig. 4 Results for the screened gap in neutron matter as a function of the Fermi momentum k_F at different steps of the screening calculations of Ref. [36] (**a**) and of our own calculations [37,38] (**b**). See text for details

gives

$$V^{(a)} = -\frac{\pi}{2}\langle\tilde{V}\rangle^2\, \Pi^0(q/k_F)\,, \tag{4}$$

where $\Pi^0(\tilde{q})$ is the static Lindhard function [$\Pi^0(0,\tilde{q})$ in Eq. (12.46b) of [42], with m replaced by m^*] with $\tilde{q} = q/k_F$. The subsequent projecting of $V^{(a)}$ on the s wave finally amounts to averaging the Lindhard function over the angle between $\mathbf{k}$ and $\mathbf{k}'$, i.e., over q in the range $|k-k'| \le q \le k+k'$. Since $\Pi^0 < 0$, the induced interaction $V^{(a)}$ is repulsive and, therefore, reduces (screens) the bare interaction V^0. The solution of the gap equation with $V^0 + V^{(a)}$ is shown as the purple dash-dot line in Fig. 4a. We see that the screening disappears at low densities, which is easily understood since $\Pi^0 \propto k_F$ in Eq. (4).

The next step is to include also diagram (b) of Fig. 2. Using the Landau approximation, the residual ph interaction is approximated as $\mathcal{V} = f_0 + g_0\, \boldsymbol{\sigma}_1 \cdot \boldsymbol{\sigma}_2$, with f_0 and g_0 the Landau parameters, and thereby the RPA series can be separately summed in the $S = 0$ and $S = 1$ channels, where S denotes the total spin of the ph excitation. Then, the inclusion of diagram (b) modifies Eq. (4) to

$$V^{(a)} + V^{(b)} = -\frac{\pi}{2}\langle\tilde{V}\rangle^2 \left(\frac{3}{2}\Pi_{S=1} - \frac{1}{2}\Pi_{S=0}\right)\,, \tag{5}$$

with

$$\Pi_{S=0} = \frac{\Pi^0}{1 - f_0\Pi^0}\,, \qquad \Pi_{S=1} = \frac{\Pi^0}{1 - g_0\Pi^0}\,. \tag{6}$$

Notice that, in dilute neutron matter, $g_0 > 0$ and $f_0 < 0$. Together with $\Pi^0 < 0$, this implies that, with increasing density, the RPA enhances the attractive $S = 0$ contribution in Eq. (5), while it reduces the repulsive $S = 1$ contribution. The net effect of diagram (b) is, therefore, that the gap (green solid line in Fig. 4a) is much less screened than with diagram (a) only.

To obtain the final result of Ref. [36], another effect was taken into account. Namely, the energy dependence of the self-energy $\Sigma(k,\omega)$ computed in Brückner theory (Fig. 1(b) of [43]) leads to a reduction of the quasiparticle weight $Z(k) = 1/(1 - \partial\Sigma/\partial\omega)$. This effect can be accounted for by introducing a factor of $Z(k)Z(k')$ on the right-hand side of the gap equation (1), which then yields the final result shown in Fig. 3 and in Fig. 4a as the blue dashed lines.

In spite of the reasonable agreement with the QMC results at high density, the increase of the gap at low-densities ($k_F \lesssim 0.27\,\mathrm{fm}^{-1}$) looks somewhat suspicious. Furthermore, besides the approximation of $\tilde{V}$ by its average $\langle\tilde{V}\rangle$ mentioned above, Ref. [36] used the Babu-Brown theory [44] to determine the Landau parameters in a self-consistent way, with the aim to avoid the liquid–gas instability in low-density symmetric nuclear matter. However, the validity of this argument may be questioned as the liquid–gas instability exists.

For these reasons, the screening problem was reconsidered by the authors in Refs. [37,38]. As input nn interaction, $V^0(k,k')$ in Eq. (2), as well as in the antisymmetrized 3p1h vertices, we use $V_{\mathrm{low}\,k}$. For the ph interaction in the RPA, as well as in the calculation of the effective mass m^*, we use for simplicity a phenomenological Skyrme energy-density functional (SLy4 in the present example). No further approximations are made, and in particular, the full momentum dependence of the 3p1h vertices is taken into account when summing over the loop momenta.

Starting with diagram (a) in Fig. 2, computed with the $V_{\mathrm{low}\,k}$ interaction obtained for a common choice of the cutoff $\Lambda = 2\mathrm{fm}^{-1}$, one obtains the gap shown in Fig. 4b as the black dashed line. As already observed in [35,36], the screening vanishes and the BCS result is recovered in the limit $k_F \to 0$, in contradiction to the GMB result. In fact, the GMB result [31] is also based on diagram (a) (since all other diagrams can be neglected in the limit $k_F a \to 0$), but with a subtle difference: In the 3p1h vertices, one has to use the scattering length (i.e., the full T matrix), and not just the bare interaction V used in diagram (a). This amounts to implicitly summing ladders to all orders in the 3p1h vertices, as shown in diagram (a′).

Making use of the RG flow of the $V_{\mathrm{low}\,k}$ interaction, a simple way to solve this problem was suggested in Ref. [37]. First, notice that, when decreasing the cut-

off Λ, the RG flow guarantees that the scattering length a_{nn} remains constant by increasing the matrix elements of the interaction as $V \approx (m/a - 2m\Lambda/\pi)^{-1}$. In this way, the interaction becomes more and more perturbative in the sense that the Born term is already a good approximation to the full T matrix. Second, the RG evolution of $V_{\mathrm{low}\,k}$ leaves the BCS gap independent of the cutoff Λ, as long as $\Lambda \gtrsim 2.5k_{\mathrm{F}}$. So, it is preferable to scale the cutoff with k_{F}, using at each density the lowest permissible cutoff $\Lambda = 2.5k_{\mathrm{F}}$. Calculating diagram (a) of Fig. 2 with this prescription, one obtains the result shown in Fig. 4b as the purple dash-dotted line, which indeed reproduces the GMB result (black star) in the limit $k_{\mathrm{F}} \to 0$.

At higher densities, the RPA corrections (Fig. 2b) become important. In the case that the ph interaction is of the Skyrme type, it is rather straightforward to resum the RPA bubble series exactly [38,45,46]. This gives our final result shown as the red dotted lines in Figs. 3 and 4b. As discussed above, the inclusion of Fig. 2b strongly reduces the screening effect of diagram (a).

If we use in diagram (b) instead of the full RPA the Landau approximation, as it was done in Refs. [35–37,47], we obtain the green solid line shown in Fig. 4b. Comparing this result with the red dashed line, one concludes that the Landau approximation is only valid for $k_{\mathrm{F}} \lesssim 0.4\mathrm{fm}^{-1}$. Beyond this density, it overestimates the effect of the RPA and, for $k_{\mathrm{F}} > 0.7\mathrm{fm}^{-1}$, it even predicts anti-screening (i.e., the gap is enhanced) because of the large values of the Landau parameters. Anti-screening was already found long ago in Ref. [33], but only at much higher densities ($k_{\mathrm{F}} \gtrsim 1.3\mathrm{fm}^{-1}$). The strong anti-screening effect found in [37] within the Landau approximation at higher density is absent or strongly suppressed within the full RPA calculation [38].

So far we have concentrated only on the low-density region with $k_{\mathrm{F}} < 0.9\mathrm{fm}^{-1}$. At higher densities, as we have seen in Sect. 2.1, the effective mass m^* leads to large uncertainties. Similarly, for the screening diagram (b), uncertainties arise from the Landau parameters f_0 and g_0 and more generally, if one goes beyond the Landau approximation, from the ph residual interactions. Hence, in [38], we repeated the calculations with a couple of different Skyrme parametrizations. All screened results shown in Fig. 5a (thick lines) were computed with the full RPA and with the density-dependent cutoff $\Lambda = 2.5\,k_{\mathrm{F}}$ for $k_{\mathrm{F}} < 0.8\mathrm{fm}^{-1}$, while we kept $\Lambda = 2\mathrm{fm}^{-1}$ constant for $k_{\mathrm{F}} \geq 0.8\mathrm{fm}^{-1}$ since this cutoff gives the correct BCS gap in the whole density range, and with larger values of Λ the advantage of the soft $V_{\mathrm{low}\,k}$ interactions would be lost. Surprisingly, when screening is included, the dependence on the choice of the Skyrme interaction is weaker than without screening. In particular, for all the considered Skyrme forces, the maximum of the screened gap lies now between 2.3 and 2.5 MeV.

These results can be compared with a calculation based on the self-consistent Green's function theory [47]. Here, the energy- and momentum-dependent single-particle self-energy $\Sigma(k,\omega)$ is computed in ladder approximation, whereby all propagators are themselves dressed ones. This approach accounts automatically for the short-range correlations created by the realistic (hard) nn interactions, but not for screening, which corresponds to long-range correlations. In Ref. [47], screening was in fact only included in an approximate way, by adding $V^{(a)} + V^{(b)}$ using the same approximations as in Ref. [36] (see above). The results, obtained with three different bare nn interactions (AV18, CDBonn, and the chiral N3LO interaction) are shown in Fig. 5b. As long as only screening is included (red, green and blue points), the maximum of the gap is again about 2.5 MeV, but the density where it tends to zero is clearly higher than in our screening calculations (Fig. 5a). However, one should keep in mind that for the momentum transfers needed in this density region neither the Landau approximation nor the full Skyrme ph interaction can be considered to be reliable.

The effect of short-range correlations is closely related to the Z factors included in the gap equation in Ref. [36]. However, using the full spectral functions as done in [47] and not just the quasiparticle peak, it becomes somewhat more sophisticated. Taking into account the short-range correlations in addition to the screening (black, purple, and turquoise points in Fig. 5b), the maximum gap is further reduced to $\approx$ 1.8 MeV. Another observation is that also the density where the $^1S_0$ gap goes to zero is reduced. Apparently this effect is important and should be studied also at lower densities, along with a more complete treatment of the screening. Short-range correlations can also be included via the correlated basis function method that once again leads to a suppression of the BCS gap [48], but this technique will not be discussed in this short review.

2.3 BCS–BEC Crossover

The BCS–BEC crossover has attracted a lot of attention in the last two decades, especially because of its experimental realization in ultracold trapped atoms. In these experiments, one can change the interatomic interaction by varying the magnetic field, in such a way that the system passes continuously from a BCS superfluid in the case of weakly attractive interactions, through a resonance where the scattering length a diverges (unitary limit), to a Bose–Einstein condensate (BEC) of bound dimers. For recent reviews emphasizing the analogies between ultracold atoms and nuclear and neutron matter, see [49,50].

Of course, in nuclear systems, the interaction cannot be changed. In this case, the crossover can be realized with changing density. Very dilute symmetric nuclear matter will form a BEC of deuterons which, with increasing density, goes continuously over into a BCS state with pn Cooper pairs [51]. In neutron matter, however, a BCS–BEC crossover does not exist, because

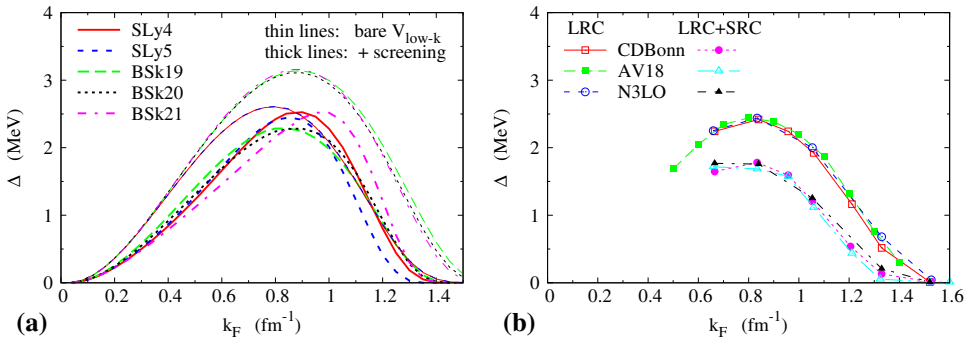

Fig. 5 Behavior of the singlet gap Δ versus k_F. **a** Results of Ref. [38] with (thick lines) and without (thin lines) medium polarization corrections for different Skyrme parameterizations used in the effective mass and in the RPA bubble summation. **b** Results of Ref. [47] including effects of medium polarization (= long-range correlations, LRC) as well as short-range correlations (SRC)

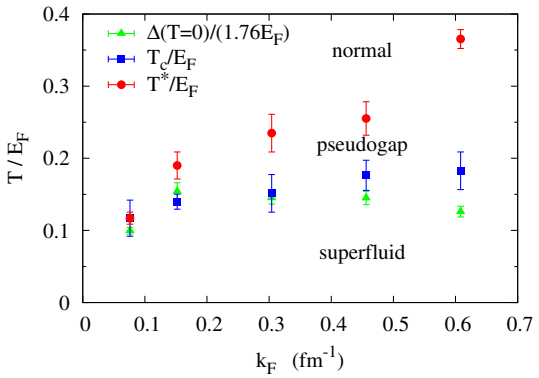

Fig. 6 QMC phase diagram of Ref. [40] displaying the critical temperature T_c (blue squares) and the pair dissociation temperature T^* (red points) in units of the Fermi energy $E_F = k_F^2/(2m)$ versus k_F. For comparison, the critical temperatures one would get from the BCS relation $T_c = 0.57\Delta(T = 0)$ are shown, too (green triangles)

there is no bound dineutron state. But the *nn* scattering length is unusually large in the *s* wave, signaling a nearly bound state. Hence, the Cooper pairs in dilute neutron matter have a relatively small size (coherence length), comparable to the average distance between particles [52,53].

In this case, similar to the situation when there is a true bound state, the temperature T^* where pairs dissociate can be higher than the superfluid critical temperature T_c where the pairs undergo Bose–Einstein condensation. This can be seen in Fig. 6 which shows the QMC results of Ref. [40] for T^* and T_c as functions of k_F. For a better visibility of the low-density results, we have divided T^* and T_c by the Fermi energy $E_F = k_F^2/(2m)$. The region between T_c and T^* is called the pseudogap phase because, although there is no true gap, there exists a suppression of the level density at $\omega = 0$ (energy measured relative to the chemical potential μ) because of the energy needed to break a pair.

In the pseudogap region, it is usually a bad approximation to compute the density from the uncorrelated occupation numbers

$$n_{\text{free}} = 2 \int \frac{d^3k}{(2\pi)^3} f(\xi(\mathbf{k}))\,, \tag{7}$$

where the factor of 2 accounts for the spin degeneracy and $f(\xi) = 1/(e^{\xi/T} + 1)$ is the Fermi function. Taking into account the density corresponding to the correlated pairs is crucial to get the correct result for T_c in the BEC limit. This is done by the Nozières-Schmitt-Rink (NSR) approach [54], which writes

$$n = n_{\text{free}} + n_{\text{corr}}\,. \tag{8}$$

The correlated density n_{corr} is calculated to first order in the self-energy Σ (in the imaginary time formalism [42]),

$$n_{\text{corr}} = 2 \int \frac{d^3k}{(2\pi)^3} \frac{1}{\beta} \sum_{\omega_n} \left(\mathcal{G}_0(\mathbf{k}, \omega_n)\right)^2 [\Sigma(\mathbf{k}, i\omega_n) - \text{Re}\,\Sigma(\mathbf{k}, \xi(\mathbf{k})]\,, \tag{9}$$

where ω_n are the Matsubara frequencies and $\mathcal{G}_0$ is the uncorrelated single-particle Green's function. The self-energy Σ is calculated within the ladder approximation as shown in Fig. 7a, b. In the original NSR paper [54], the correlated density is obtained as the derivative with respect to μ of the thermodynamic potential represented by diagram (c) in Fig. 7, which is equivalent to keeping the self-energy only to first order in Eq. (9) [49]. However, the subtraction of the on-shell self-energy $\Sigma(\mathbf{k}, \xi(\mathbf{k}))$ in Eq. (9) is absent in the original NSR approach. It is necessary as this term is already taken into account in $\mathcal{G}_0$ via the quasiparticle energy [55–58].

The correlated density was calculated in [58] using the $V_{\text{low}\,k}$ interaction. To accommodate the non-local interaction, the authors expressed the correlated density in the basis that diagonalizes $V\bar{G}_0^{(2)}$, where $\bar{G}_0^{(2)}$ is the two particle retarded Green's function. In [37,38] the bare interaction was augmented by the induced

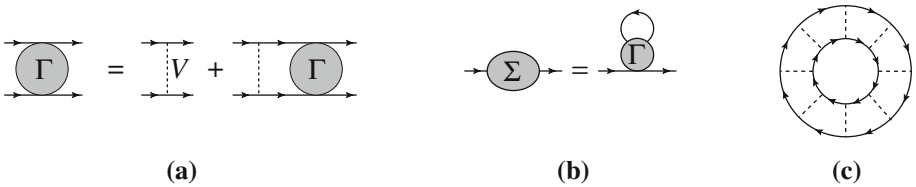

Fig. 7 Diagrams for the T matrix (**a**), the self-energy (**b**), and the thermodynamic potential (**c**) in ladder approximation

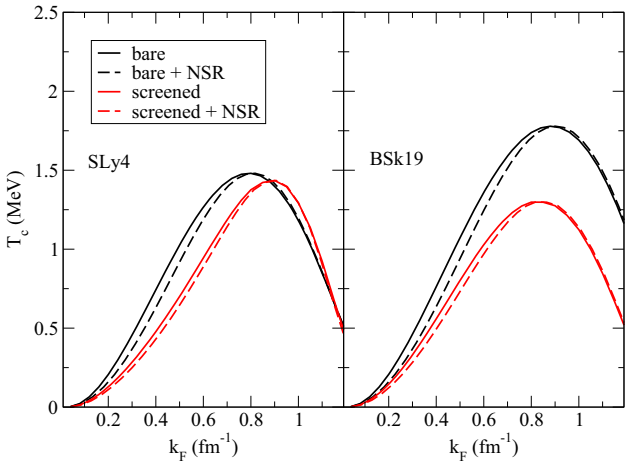

Fig. 8 Critical temperature T_c with (red) and without (black) screening corrections, as a function of k_F computed with (dashes) and without (solid lines) the NSR correction to the density, for two different Skyrme parmetrizations used in the calculation of the effective mass and of the screening corrections $V^{(a)} + V^{(b)}$ [38]

interaction as discussed in Sect. 2.2. A similar calculation using a separable interaction instead of $V_{\text{low}\,k}$, but without screening corrections, was done in [59]. In all these calculations, the subtraction term was approximated by the first-order Hartree–Fock (HF) self-energy. For a detailed comparison of different subtraction prescriptions, see [60].

Figure 8 shows the effect of including the correlated density on the density dependence of the transition temperature [38]. The black lines include the effective mass m^*, computed with SLy4 (left panel) and BSk19 (right panel), while the red lines include also the screening effects $V^{(a)}+V^{(b)}$ (calculated with the same Skyrme force as m^*). For the solid lines, k_{F} was computed with n_{free}, while for the dashed lines, k_{F} was computed with the NSR density $n_{\text{free}} + n_{\text{corr}}$. We note that the effect of screening overwhelms the effect of NSR and, hence, the change in the transition temperature. In particular, with screening included, the NSR effect is even smaller than with the bare interaction.

The smallness of the NSR effect is consistent with the fact that the QMC critical temperature T_c of Ref. [40] satisfies well the BCS relation $T_c \approx 0.57\Delta(T=0)$ as can be seen in Fig. 6. Also, the pseudogap computed in [60] is very small. Therefore, it is surprising that the temperatures T^* up to which pair correlations survive in Ref. [40] can be quite far above T_c.

3 Triplet pairing

Pairing in the triplet channel is supposed to occur at much higher densities, say, $k_{\text{F}} \gtrsim 1.3\text{fm}^{-1}$ (corresponding to number densities $n \gtrsim 0.07$ fm^{-3} or mass densities $\rho \gtrsim 1.2\times10^{14}$g/cm^3), and hence occurs in the outer layers of the neutron star core. The evidence for pairing in the spin-triplet channel at high densities comes from the fact that for momenta $\gtrsim 1.3\,\text{fm}^{-1}$, the attraction in this channel gets stronger, resulting in positive two-body phase shifts (see left panel of Fig. 9), until it becomes the most attractive channel that supports pairing at high densities [62]. In the spin-triplet channel, due to the tensor force, the $l=1$ and $l=3$ partial waves are coupled, with total angular momentum $J=2$, and it is denoted as ${}^3P_2 - {}^3F_2 \equiv {}^3PF_2$. The zero-temperature BCS gap is obtained by solving the angle-averaged gap equation [63] that couples the $l = J \pm 1$ states and is written as,

$$\Delta_l(k) = -\sum_{l'} \frac{(-1)^{(l-l')/2}}{\pi} \int_0^\infty q^2 dq V_{ll'}(k,q) \frac{\Delta_{l'}(q)}{E(q)}, \tag{10}$$

where $E(q) = \sqrt{\xi^2(q) + D^2(q)}$ and $\xi(q) = \varepsilon(q) - \mu$. Further, the overlap between the different partial waves is ignored and $D^2(q) = \Delta_1^2(q) + \Delta_3^2(q)$ [62,63]. The validity of the angle-averaging approximation was confirmed in [64].

However, pairing in this channel is plagued by uncertainties as the input free-space two-body interactions, which are the starting point for the BCS gap equation, are not phase shift equivalent [47,63,65–69]. This is seen in Fig. 9a, where the phase shifts and mixing angle are compared against the experimental phase shift [61] for two representative realistic interactions, the phenomenological interaction, AV18 [70] and the chiral interaction at N3LO [71], as a function of lab energies. From Fig. 9a, it is seen that beyond lab energies of ≈ 150 MeV, the agreement is rather poor. These discrepancies result in model-dependent gaps already at the BCS level as seen in Fig. 9b.

While [63] used realistic interactions to track the model dependence at the BCS level in the triplet pairing gaps, the input interactions used in [65–67], are the modern NN interaction obtained via chiral perturbation theory at N3LO which are further softened by the RG running [23]. The similarity renormalization group (SRG) interactions (V_{srg}) are very useful in studying the gaps in the spin triplet channel. For a given bare interaction, such as AV18 [70] or N3LO [71], the SRG evo-

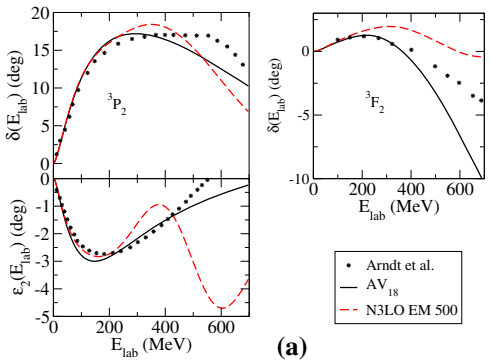

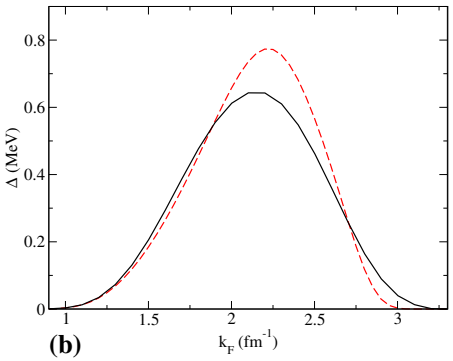

Fig. 9 Phase shifts and mixing in the ${}^3PF_2$ channel against the experimental phase shift of Arndt et al. [61]. Beyond lab energies of ~ 150 MeV, the phase shifts from the AV18 and N3LO do not agree with the experimental phase shifts. This is reflected in a model-dependent gap in at the BCS level. It should be noted that the N3LO results for k_F beyond $2.5\,\mathrm{fm}^{-1}$ becomes unreliable as the chiral cutoff $\Lambda \sim 3.0\,\mathrm{fm}^{-1}$

lution preserves the phase shifts at all energies (unlike $V_{\mathrm{low}\,k}$ which preserves the phase shifts only for $k < \Lambda$) and hence, the variation of the gap as a function of the SRG evolution scale λ quantifies the missing $3N$ force and medium corrections, and, has nothing to do with the inequivalence of the phase shifts [66]. In a complementary study, the authors of [65], analyzed the dependence of the gap on the chiral cutoff when the N3LO interactions were used as inputs, which highlights the differences in dealing with the two pion exchange interaction term (see Fig. 9 in [65]).

The correlations beyond the BCS approximation correct both the quasiparticle spectrum and the particle–particle vertex that enters the gap equation. The first-order Hartree–Fock self-energy is given by,

$$\Sigma^{(1)}(k) = \int \frac{d^3k'}{(2\pi)^3}\, n_{\mathbf{k}'} \sum_{l,S,J} 2\pi(2J+1) \langle q|V_{SlJ}|q\rangle(1-(-1)^{l+S+1}), \qquad (11)$$

where $n_{\mathbf{k}} = \theta(k_F - k)$ is the Fermi–Dirac distribution at zero temperature and $q = |\mathbf{k} - \mathbf{k}'|/2$. The HF self-energy changes the free quasiparticle spectrum to $\varepsilon(k) = k^2/(2m^*) + \Sigma^{(1)}(k)$, and $k_F/m^* = [d\varepsilon(k)/dk]_{k=k_F}$ relates the effective mass to the self-energy. When $m^* < m$, the density of states near the Fermi surface decreases and, hence, one can expect a suppression of pairing and therefore, smaller gaps.

Figure 10 shows the gaps with both the free single particle spectrum (lines) and with the effective mass m^* (symbols—circles and squares). The black solid line is the bare interaction and the dashed lines and dash-dotted lines are the gaps obtained from the SRG evolved interactions for $\lambda = 2.0\,\mathrm{fm}^{-1}$ and $2.5\,\mathrm{fm}^{-1}$, respectively. The filled circles are the results for the gap with effective mass calculated from the Brückner Hartree–Fock (BHF) by Baldo et al. [63]. The squares, filled and empty are the first-order effective mass calculated using Eq. (11) for $\lambda = 2.5\,\mathrm{fm}^{-1}$ and $2.0\,\mathrm{fm}^{-1}$ respectively. When compared with the free single particle spectrum, the inclusion of the effective mass, both

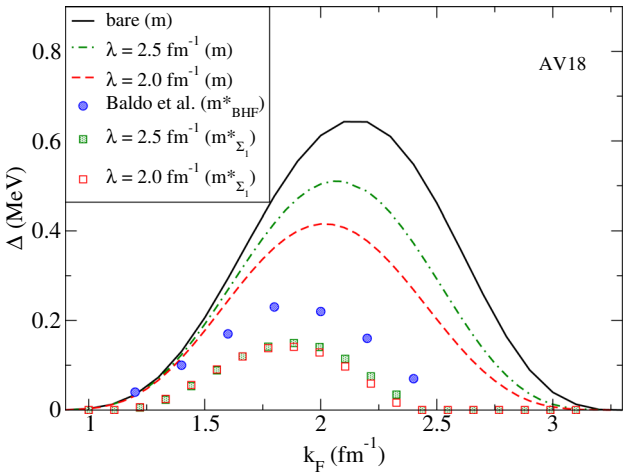

Fig. 10 Medium effects: Comparing the gaps with free single particle spectrum (lines) and effective mass (symbols) for the AV18 interaction. The blue dots are the results of Baldo et al [63] and the squares show the gaps computed with V_{srg} for $\lambda = 2.5\,\mathrm{fm}^{-1}$ (green filled squares) and $\lambda = 2.0\,\mathrm{fm}^{-1}$ (red empty squares) respectively

BHF and first order, reduces the gaps, due to the suppression of the density of states at k_F. However, the gaps are more suppressed with a first-order effective mass compared to the effective mass from BHF. This should be expected at high densities, as a first order calculation of the self-energy is insufficient. It is interesting to note that the dependence on λ is dramatically lessened with an effective mass when compared to the corresponding free spectrum result. Lowering λ makes the SRG evolved interaction more attractive and hence increases the effective mass. However, including an effective mass reduces the BCS gap. The dramatic decrease in the λ dependence arises due to a compensation between these two effects.

The three-body force is expected to play a crucial role for pairing in the triplet channel and in fact enhances the gap [65–67,69,72,73]. These forces have been calculated microscopically using semi-phenomenological

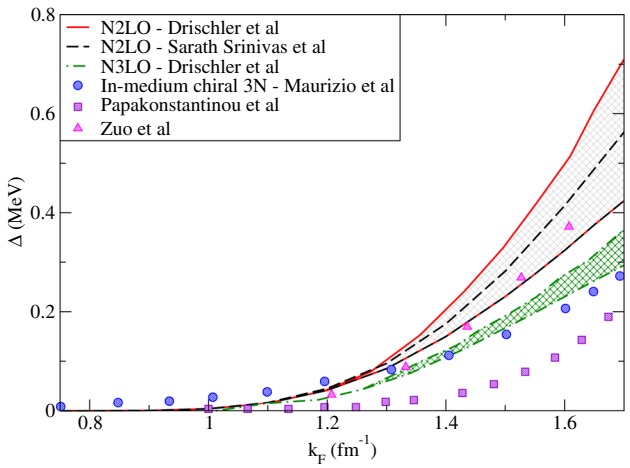

Fig. 11 Triplet gaps including $3N$ interactions from Drischler et al. [67], Srinivas et al. [66], Maurizio et al. [65], Papakonstantinou et al. [69], and Zuo et al. [68]

interactions [68,69,72,74] as well as using chiral EFT, where the $3N$ terms first enter at N2LO [73,75]. Figure 11 shows the triplet gap including the $3N$ interaction, which is usually incorporated as a density-dependent $2N$ interaction. While in [65], the density-dependent $2N$ interaction is generated from an in-medium chiral $3N$ force, Refs. [66,67] use an effective density-dependent $2N$ interaction from the $3N$ chiral interactions at N2LO [73]. In addition, [67] also considers the $3N$ contributions from N3LO. In Fig. 11, the area shaded in gray between the solid red lines represents the variations in the gap due to the uncertainties in the low-energy constants [67] as well as the three-body cutoff, while the black dashed lines represent the effect of varying the three-body cutoff after fixing the chiral low-energy constants [66]. The green hatched region between the dash-dotted green lines represents the gaps obtained with $3N$ interactions at N3LO with the associated uncertainties in the low-energy constants [67]. It is worth noting that the spin triplet gaps are extremely sensitive to the three-body force compared to the spin singlet gap [67,69,73]. In the $^1S_0$ channel the corrections to the gap enter only at higher densities, while in the $^3PF_2$ channel, the effects of the three-body interaction on the gap are dramatic.

As discussed already in Sect. 2.2, beyond BCS correlations (short and long range) lead to important modifications of the gap. The literature on including these medium effects for the p-wave is rather sparse, with some recent attempts by Dong et al [76] and Ding et al [47]. The authors in [76], calculate the quasiparticle weight Z as was done in [36] for the singlet channel (see Sect. 2.2). The quasiparticle weight was calculated both with and without the inclusion of a three-body force. The presence of the Z factor suppresses the gaps by an entire order of magnitude as well as shrinks the density region where the gaps exist. In [47], the short-range correlations are taken into account via the self-consistent Green's function techniques, extrapolated to zero temperatures. In addition, the screening corrections as in [36] (see Sect. 2.2) have been extended to the p-wave. In this case it seems that the screening enhances the gap (antiscreening) while the short-range correlations suppress it, with the net effect of strongly reducing the gaps compared to the BCS results.

While pairing in the triplet channel is an important ingredient to describe the physics of the neutron star core, much remains to be explored due to the uncertainties in the free-space interactions.

4 Conclusions

In this brief review, we discussed the state of the art concerning the s and p-wave pairing in pure neutron matter. In the s-wave, which is most relevant at low densities, the gap as a function of density seems to be under control. QMC and the most recent many-body calculations agree that the gap, before reaching a maximum of $\sim 2-2.5$ MeV at $k_F \sim 0.8\,\mathrm{fm}^{-1}$, follows the behavior of the BCS gap reduced by a factor of 0.6–0.7, except at extremely low densities (of purely academic interest) where the GMB (reduction by a factor of 0.45) limit is reproduced. Effects of BCS–BEC crossover on the critical temperature seem to be very weak. Beyond the maximum of the gap, there are uncertainties that come from medium effects such as effective mass, screening and short-range correlations. In addition, there are other factors such as $3N$ forces that are important at higher-densities, which we have not discussed here.

In the p-wave, which is supposed to be dominant at high densities, even at the BCS level, the gaps have large uncertainties. Inclusion of short- and long-range correlations seem to reduce the gaps while the $3N$ force enhances it. However, since the p-wave is always in the extremely weak coupling limit, the gaps exhibit exponential sensitivity to the details of the interactions and the approximations. At densities corresponding to the neutron star core, it would be more realistic to consider asymmetric matter with a finite proton fraction. This might completely change the conclusions through the nnp $3N$ interactions.

Acknowledgements The authors acknowledge support from Collaborative Research Program of IFCPAR/CEFIPRA, Project number: 6304-4.

Author contribution statement

Both authors contributed equally to this work.

References

1. A.B. Migdal, Zh. Eksp, Teor. Fiz. **37**, 249 (1959) [Sov. Phys. JETP **10**, 176 (1960)]

2. A.B. Migdal, Nucl. Phys. **13**, 655 (1959)
3. V.L. Ginzburg, D.A. Kirzhnits, Zh. Eksp, Teor. Fiz. **47**, 2006 (1964) [Sov. Phys. JETP **20**, 1346 (1965)]
4. J. Bell, A. Hewish, J.D.H. Pilkington, P.F. Scott, R.A. Collins, Nature **217**, 709 (1968)
5. T. Gold, Nature **218**, 731 (1968)
6. G. Baym, C.J. Pethick, D. Pines, M. Ruderman, Nature **224**, 872 (1969)
7. D. Pines, M.A. Alpar, Nature **316**, 27 (1985)
8. N. Andersson, K. Glampedakis, W.C.G. Ho, C.M. Espinoza, Phys. Rev. Lett. **109**, (2012)
9. D.G. Yakovlev, C.J. Pethick, Ann. Rev. Astron. Astrophys. **42**, 169 (2004)
10. D. Page, J.M. Lattimer, M. Prakash, A.W. Steiner, Astrophys. J. **707**, 1131 (2009)
11. P.W. Anderson, N. Itoh, Nature **256**, 25 (1975)
12. A. Bohr, B.R. Mottelson, D. Pines, Phys. Rev. **110**, 936 (1958)
13. A. Bohr, B.R. Mottelson, *Nuclear Structure*, vol. 1 (Benjamin, New York, 1959)
14. D.Q. Fang et al., Phys. Rev. C **6**(9), 034613 (2004)
15. A. Ozawa et al., Nucl. Phys. A **691**, 599 (2001)
16. K. Hagino, H. Sagawa, Phys. Rev. C **84**, 011303 (2011)
17. N. Chamel, P. Haensel, Liv. Rev. Relativ. **11**, 10 (2008)
18. D.J. Dean, M. Hjorth-Jensen, Rev. Mod. Phys. **75**, 607 (2003)
19. B. Haskell, A. Sedrakian, in: L. Rezzolla, P. Pizzochero, D. Jones, N. Rea, I. Vida na (eds.) *The Physics and Astrophysics of Neutron Stars*. Astrophysics and Space Science Library, Vol. 457 (Springer, Cham, 2018)
20. A. Sedrakian, J.W. Clark, Eur. Phys. J. A **55**, 167 (2019)
21. J.R. Schrieffer, *Theory of Superconductivity* (Benjamin, New York, 1964)
22. S.K. Bogner, R.J. Furnstahl, S. Ramanan, A. Schwenk, Nucl. Phys. A **784**, 79 (2007)
23. S. Bogner, R. Furnstahl, A. Schwenk, Prog. Part. Nucl. Phys. **65**, 94 (2010)
24. K. Hebeler, A. Schwenk, B. Friman, Phys. Lett. B **648**, 176 (2007)
25. M. Buraczynski, N. Ismail, A. Gezerlis, Phys. Rev. Lett. **122**, 152701 (2019)
26. J. Dechargé, D. Gogny, Phys. Rev. C **21**, 1568 (1980)
27. F. Chappert, M. Girod, S. Hilaire, Phys. Lett. B **668**, 420 (2008)
28. E. Chabanat, P. Bonche, P. Haensel, J. Meyer, R. Schaeffer, Nucl. Phys. A **635**, 231 (1998)
29. N. Chamel, S. Goriely, J.M. Pearson, Phys. Rev. C **80**, 065804 (2009)
30. S. Goriely, N. Chamel, J.M. Pearson, Phys. Rev. C **82**, 035804 (2010)
31. L. P. Gor'kov, T.K. Melik-Barkhudarov, Zh. Eksp. Teor. Fiz. **40**, 1452 (1961) [Sov. Phys. JETP **13**, 1018 (1961)]
32. J. Wambach, T.L. Ainsworth, D. Pines, Nucl. Phys. A **555**, 128 (1993)
33. H.J. Schulze, J. Cugnon, A. Lejeune, M. Baldo, U. Lombardo, Phys. Lett. B **375**, 1 (1996)
34. C. Shen, U. Lombardo, P. Schuck, Phys. Rev. C **67**, 061302 (2003)
35. C. Shen, U. Lombardo, P. Schuck, Phys. Rev. C **71**, (2005)
36. L.G. Cao, U. Lombardo, P. Schuck, Phys. Rev. C **74**, 064301 (2006)
37. S. Ramanan, M. Urban, Phys. Rev. C **98**, 024314 (2018)
38. M. Urban, S. Ramanan, Phys. Rev. C **101**, 035803 (2020)
39. S. Gandolfi, AYu. Illarionov, S. Fantoni, F. Pederiva, K.E. Schmidt, Phys. Rev. Lett. **101**, 132501 (2008)
40. T. Abe, R. Seki, Phys. Rev. C **79**, 054002 (2009)
41. A. Gezerlis, J. Carlson, Phys. Rev. C **81**, 025803 (2010)
42. A.L. Fetter, J.D. Walecka, *Quantum Theory of Many-Particle Systems* (McGraw-Hill, New York, 1971)
43. M. Baldo, A. Grasso, Phys. Lett. B **485**, 115 (2000)
44. S.V. Babu, G.E. Brown, Ann. Phys. (N.Y.) **77**, 1 (1973)
45. C. García-Recio, J. Navarro, Van Giai Nguyen, L.L. Salcedo, Ann. Phys. (N.Y.) **214**, 293 (1992)
46. A. Pastore, D. Davesne, J. Navarro, Phys. Rep. **563**, 1 (2015)
47. D. Ding, A. Rios, H. Dussan, W.H. Dickhoff, S.J. Witte, A. Carbone, A. Polls, Phys. Rev. C **94**, 025802 (2016)
48. G.E. Pavlou, E. Mavrommatis, C. Moustakidis, J.W. Clark, Eur. Phys. J. A **53**, 96 (2017)
49. G. Calvanese Strinati, P. Pieri, G. Röpke, P. Schuck, M. Urban, Phys. Rep. **738**, 1 (2018)
50. Y. Ohashi, H. Tajima, P. van Wyk, Prog. Part. Nucl. Phys. **111**, 103739 (2020)
51. M. Baldo, U. Lombardo, P. Schuck, Phys. Rev. C **52**, 975 (1995)
52. M. Matsuo, Phys. Rev. C **73**, 044309 (2006)
53. J. Margueron, H. Sagawa, K. Hagino, Phys. Rev. C **76**, 064316 (2007)
54. P. Nozières, S. Schmitt-Rink, J. Low. Temp. Phys. **59**, 195 (1985)
55. R. Zimmermann, H. Stolz, Phys. Status Solidi B **131**, 151 (1985)
56. M. Schmidt, G. Röpke, H. Schulz, Ann. Phys. **202**, 57 (1990)
57. M. Jin, M. Urban, P. Schuck, Phys. Rev. C **82**, 024911 (2010)
58. S. Ramanan, M. Urban, Phys. Rev. C **88**, 054315 (2013)
59. H. Tajima, T. Hatsuda, P. van Wyk, Y. Ohashi, Sci. Rep. **9**, 18477 (2019)
60. D. Durel, M. Urban, Universe **6**, 208 (2020)
61. R.A. Arndt, C.H. Oh, I.I. Strakovsky, R.L. Workman, F. Dohrmann, Phys. Rev. C **56**, 3005 (1997)
62. T. Takatsuka, R. Tamagaki, Prog. Theor. Phys. Suppl. **112**, 27–66 (1993)
63. M. Baldo, Ø. Elgarøy, L. Engvik, M. Hjorth-Jensen, H.-J. Schulze, Phys. Rev. C **58**, 1921 (1998)
64. V.V. Khodel, V.A. Khodel, J.W. Clark, Nucl. Phys. A **679**, 827 (2001)
65. S. Maurizio, J.W. Holt, P. Finelli, Phys. Rev. C **90**, 044003 (2014)
66. S. Srinivas, S. Ramanan, Phys. Rev. C **94**, 064303 (2016)
67. C. Drischler, T. Krüger, K. Hebeler, A. Schwenk, Phys. Rev. C **95**, 024302 (2017)
68. W. Zuo, C.X. Cui, U. Lombardo, H.J. Schulze, Phys. Rev. C **78** (2008)
69. P. Papakonstantinou, J.W. Clark, J. Low. Temp. Phys. **189**, 361 (2017)
70. R.B. Wiringa, V.G.J. Stoks, R. Schiavilla, Phys. Rev. C **51**, 38–51 (1995)
71. D.R. Entem, R. Machleidt, Phys. Rev. C **68**, 041001 (2003)

72. X.R. Zhou, H.J. Schulze, E.G. Zhao, F. Pan, J.P. Draayer, Phys. Rev. C **70**, 048802 (2004)
73. K. Hebeler, A. Schwenk, Phys. Rev. C **82**, 014314 (2010)
74. Z.H. Li, U. Lombardo, H.-J. Schulze, W. Zuo, Phys. Rev. C **77**, 034316 (2008)
75. J.W. Holt, N. Kaiser, W. Weise, Phys. Rev. C **81**, 024002 (2010)
76. J.M. Dong, U. Lombardo, W. Zuo, Phys. Rev. C **87**, 062801 (2013)